J Mol Model (2013) 19:3307–3323
DOI 10.1007/s00894-013-1864-2

ORIGINAL PAPER

Effects of local protein environment on the binding of diatomic molecules to heme in myoglobins. DFT and dispersion-corrected DFT studies

Meng-Sheng Liao · Ming-Ju Huang · John D. Watts

Received: 15 November 2012 / Accepted: 18 April 2013 / Published online: 10 May 2013

Abstract The heme-AB binding energies (AB = CO, O_2) in a wild-type myoglobin (Mb) and two mutants (H64L, V68N) of Mb have been investigated in detail with both DFT and dispersion-corrected DFT methods, where H64L and V68N represent two different, opposite situations. Several dispersion correction approaches were tested in the calculations. The effects of the local protein environment were accounted for by including the five nearest surrounding residues in the calculated systems. The specific role of histidine-64 in the distal pocket was examined in more detail in this study than in other studies in the literature. Although the present calculated results do not change the previous conclusion that the hydrogen bonding by the distal histidine-64 residue plays a major role in the O_2/CO discrimination by Mb, more details about the interaction between the protein environment and the bound ligand have been revealed in this study by comparing the binding energies of AB to a porphyrin and the various myoglobins. The changes in the experimental binding energies from one system to another are well reproduced by the calculations. Without constraints on the residues in geometry optimization, the dispersion correction is necessary, since it improves the calculated structures and energetic results significantly.

Keywords Carbon monoxide · DFT calculations · Dispersion correction · Myoglobins · Oxygen

Electronic supplementary material The online version of this article (doi:10.1007/s00894-013-1864-2) contains supplementary material, which is available to authorized users.

M.-S. Liao · M.-J. Huang · J. D. Watts (✉)
Department of Chemistry, Jackson State University, Jackson, MS 39217, USA
e-mail: john.d.watts@jsums.edu

Introduction

Myoglobin (Mb) and hemoglobin (Hb) are hemoproteins whose physiological importance is primarily related to their ability to bind molecular oxygen (O_2). Mb functions as an O_2 storage, providing O_2 to the working muscles; Hb, possessing a similar structure to Mb, functions primarily in the transport of O_2 from the lungs to the tissues of the body. Mb has been studied extensively by experiments, probably because it is relatively simple; it has often served as an example of ligand binding, control, and recognition [1]. The active center of both Mb and Hb consists of iron protoporphyrin IX (FePPIX) complex bound through a single, 'proximal', axial histidine (His) to the protein. This FePPIX(His) moiety in Mb/Hb is also called *heme*. The other side of the porphyrin plane remains free to bind O_2 and other ligands. Figure 1 illustrates the familiar four-coordinate FePPIX of heme *b* and the heme group bound to O_2 within the Mb unit.

As respiratory proteins, Mb and Hb must favor the binding of O_2 compared to CO and NO to avoid suffocation; the latter two molecules are ubiquitous in biology. The binding affinity of CO to an iron porphyrin is 10^5-fold larger than that of O_2. However, this ratio is reduced by several orders of magnitude when the heme is embedded in the protein matrix [2]. Clearly, the intermolecular interactions by the surrounding protein polypeptide assist in the discrimination against endogenous CO inhibition.

The underlying mechanism of ligand discrimination in Mb has attracted much interest from both experimentalists and theorists. It was once a central point of view in the field that the bent geometry of CO observed in the previous X-ray [3] and neutron [4] crystal structures of MbCO, is the major cause of the reduced affinity for CO. This is a steric hindrance mechanism suggested by Collman et al. [2] more

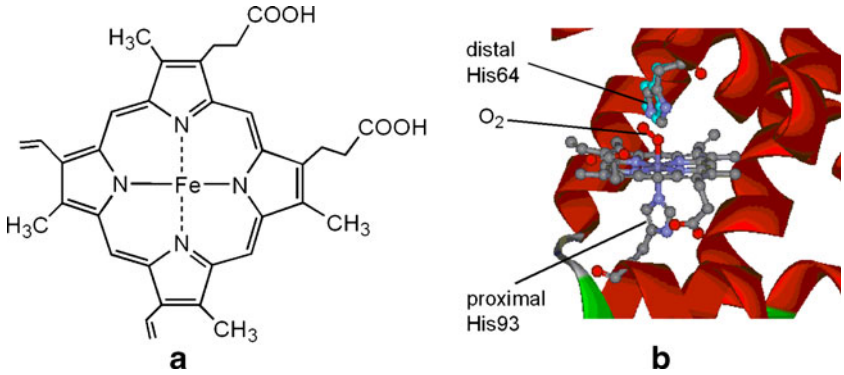

Fig. 1 **a** Iron protoporphyrin IX of hemoproteins. **b** The heme group bound to O_2 in the presence of the distal (His64) and proximal (His93) histidines within the myoglobin (Mb) (*code* 1A6M)

than 35 years ago, who argued that the strategically placed distal histidine residue (His64) in the protein pocket, positioned over Fe, could accommodate the bent O_2, but would inhibit binding of the normally upright CO. However, later X-ray crystal structures of MbCO [5, 6] show very little bending angles (relative to upright position), and sophisticated infrared experiments [7, 8] have ruled out the possibility of severe FeCO bending, as have the different computations [9, 10]. Many site-directed mutagenesis studies [11] also do not give a result consistent with this hypothesis. It is now generally accepted that the earlier structures [3, 4] and idea (a strongly bent FeCO unit as the reason for the discrimination) [2] were incorrect.

An alternative explanation of this difference is centered on a stabilizing hydrogen bond (H-bond) interaction between the distal histidine and the bound ligand (see Fig. 1b). It is suggested that the distal histidine side chain, having an acidic NH group, can H-bond more favorably with bound O_2 than with CO. This idea has been supported by neutron diffraction [12], infrared (IR) spectroscopy [10], NMR [13], and theoretical [14, 15] studies, which demonstrated an important influence of polarity on the binding of O_2, but not CO, to the heme group.

There have been many theoretical studies of the interaction of AB (AB = CO, O_2, NO) with a *model* heme. Iron porphine (FeP) with an axial ligand L such as imidazole (Im), pyridine (Py), or NH_3 has been used to mimic the heme. Its AB complex FeP(L)(AB) is therefore used as model for heme(AB). Very early theoretical studies (e.g., refs. [16–19]) were performed with semiempirical, Hartree-Fock, or X_α methods at a fixed geometry. Those studies were limited to a qualitative analysis based on orbital energies, populations, and atomic charge distributions, etc. Later, density functional theory (DFT) methods have been applied to FeP(L)(AB) (e.g., refs. [14, 15, 20–33]). Several recent DFT studies [14, 15, 25–28, 31, 33] have included the protein environment in the calculations. Spiro and coworkers [27] considered a large heme(AB) model system that includes the 13 closest, surrounding residues. They compared Mb to H64I, but just reported the relative energies between Mb-AB and H64I-AB (AB = CO, O_2) (see Experimental data and previous calculated results section). Strickland et al. [28] calculated the Fe-CO binding energy in MbCO with a quantum mechanics/molecular mechanics (QM/MM) method; Mb was shown to weaken the Fe-CO bond by 5.8 kcal mol^{-1}, which is significantly larger than experiment (~1.15 kcal mol^{-1}, see Experimental data and previous calculated results section). Shaik and co-workers [31] performed a QM/MM study of MbO_2, focusing mainly on the effects of the protein on the nature of the Fe-O_2 bonding. In the previous QM/MM calculations [14, 15, 25, 28, 31], the QM region included at most one residue (His64) in addition to FeP(Im)(AB), thereby neglecting the polarization effects from other surrounding residues and the strain energy stored in the protein itself [33]. More recently, Cole et al. [33] used a rather approximate linear-scaling DFT + U method to investigate the ligand discrimination in Mb; however, the accuracy of the calculated results depends greatly on the choice of the adjustable parameter U.

Recent experimental work [34–38] in this area sought to obtain a detailed understanding of ligand binding to Hb and Mb and of the role of the surrounding protein structure. In doing so, extensive mutagenesis of the distal pockets in the globins has been carried out and a wealth of structural, kinetic, and spectroscopic information for many mutants has been obtained from experiment [34–38]. Despite several recent theoretical studies [27, 28, 33], there are still many unknowns regarding the interactions of the heme-ligand adduct with the surrounding proteins in Mb or Hb, and many details in the mutagenesis experiments [34–38] remain to be addressed. The following questions may be raised here:

(1) What is the precise interaction energy between the bound AB and the distal protein environment? This energy is unknown precisely from experiment or previous quantum chemical calculations. What is known from experiment is either the free energy of MbAB deduced from equilibrium constant data [39] or the enthalpy from calorimetry or temperature variations

of the equilibrium constant [40]. The interaction energy between bound AB and the distal histidine-64 (His64) has been evaluated with DFT methods [14, 15, 26], but the effects of the other heme pocket components on the bound AB are unknown. Thus, we have question (2):

(2) In addition to His64 (see Fig. 1b), how large is the energetic contribution from the other neighboring residues to the binding of AB to the heme? The previous DFT studies of heme(AB) that considered the protein environment have mainly included a single His64 in the calculations. The energetic contribution from the other neighboring residues has not been investigated in detail.

(3) Can the experimental kinetic data (ligand dissociation rate constant k_{AB}) for various mutants be exactly correlated with the calculated ligand binding energies [E_{bind}(AB)] for a residue substitution in the globins? There is a relationship between the change (Δ) in E_{bind}(AB) and the change in k_{AB}: $\Delta E_{AB} = kT\Delta \ln k_{AB}$ [41] (see Table 1). Although experimental studies [34–38] yield very useful information about the selectivity of Mb, it is not always possible to provide an explanation of the results obtained for the various mutants.

In this work, both DFT and dispersion-corrected DFT calculations have been carried out to investigate the heme-AB binding energies (AB = CO, O_2) in a wild-type Mb and two mutants (H64L, V68N) of Mb, where H64L and V68N represent two different, opposite situations. The His64 to leucine (Leu) substitution causes a large decrease in O_2 affinity, while there is a significant increase in O_2 affinity when the valine-68 in Mb is replaced with asparagine (Asn). It would be of interest to compare the two situations.

Although DFT has proven to be efficient in calculations on heme-AB complexes, it is argued [42–45] that the DFT methods in common use today do not properly describe the long-range dispersion interactions. This is because the present DFT methods are thought to be "local" or at most "semilocal" theories [43], even if they include gradients or higher-order derivatives; but dispersion is a long-range, nonlocal electron correlation effect. In recent years, there has been considerable interest in overcoming the lack of dispersion forces in standard DFT and a number of dispersion correction approaches have been proposed in the literature [46]. One most practical and successful approach in the field has been adding a (semi-)empirical correction of the form C_6R^{-6} to a density functional scheme to yield a DFT + E_{disp} model (it is denoted as DFT-D by some other authors [45]). Meanwhile, many modifications of the DFT + E_{disp} approach have also been made (see DFT and dispersion-corrected DFT methods section).

Recently, we assessed the performance of DFT + E_{disp} for several large biological systems [47]. Three versions of Grimme's dispersion correction methods [48] were tested; they are labeled as DFT-D1, -D2, and -D3, respectively (see DFT and dispersion-corrected DFT methods section). DFT-D1 was shown to yield structures and energetic results which are adequate. In contrast, the -D2 and -D3 approaches place the residues too close to the heme and their calculated relative binding energies are in poor agreement with experiment in most cases, but the newer -D3 version is an improvement over the old -D2 one. More recently, a revised version of DFT-D3 was reported by Grimme et al. [49]. It uses the rational damping proposed by Becke and Johnson (see DFT and dispersion-corrected DFT methods section). This variant, labeled as -D3(BJ), has been implemented in the updated ADF program. The current ADF also includes the density-dependent dispersion correction (dDsC) method developed by Steinmann and Corminboeuf [50] (see DFT and dispersion-corrected DFT methods section).

Compared to the previous work [47], many additional calculations have been performed in the present work:

(1) Considering the fact that the residues around the heme(AB) are linked to the protein backbone, constraints are imposed on the residues in the geometry optimization here. In the previous work [47], the distal residues above the heme plane were allowed to move freely in geometry optimization. A comparison is made between the results obtained with and without the constraints in geometry optimization.

(2) In addition to exploring the effects of the local protein environment in the various myoglobins, the present work examines the specific role of His64 in the distal pocket of Mb in somewhat more detail than other studies in the literature.

(3) The more recently developed -D3(BJ) and -dDsC dispersion correction methods are tested on some of the present systems.

Experimental data and previous calculated results

First of all, some comments have to be made on the experimental data for the AB binding energies to porphyrins and myoglobins. Certain relevant binding properties are presented in Table 1; they include the equilibrium constant ratio K_{CO}/K_{O2}, dissociation rate constant k_{AB}, the estimated binding energies E_{bind}(AB) [i.e., E_{bind}(Por-AB), E_{bind}(Mb-AB), etc.], and ΔE_{AB} (which is the difference of the binding energies between the wild-type Mb and the indicated mutant). Four myoglobins are given here: Mb, H64I, H64L, and V68N. In the following, we always use Mb to stand for a wild-type myoglobin, whereas the mutated Mbs are labeled with the names of the mutants themselves such as H64I, H64L, and V68N, which have the following meaning:

Table 1 Equilibrium constant ratio (K_{CO}/K_{O2}), dissociation rate constants (k, s^{-1}) (from refs. [34, 35]) and estimated binding energies (E_{bind}, eV)[a] for O_2 and CO binding to porphyrin (Por) and wild-type and mutants of sperm whale myoglobin[b]

	K_{CO}/K_{O2}	k_{CO}	k_{O2}	ΔE_{CO}[d]	ΔE_{O2}[d]	$E_{bind}(CO)$	$E_{bind}(O_2)$
Por in benzene[c]	22000	0.025	4200	0.01	0.15	0.78[h], 0.79[j]	0.53[i], 0.55[j]
Por (in vacuum)						0.85[f]	0.44[f]
Mb (wild-type)	25	0.019	15	0[e]	0[e]	0.80[g]	0.70[g]
H64I	12000	0.047	6400	0.02	0.16	0.78[j]	0.54[j]
H64L	48000	0.024	4100	0.01	0.14	0.79[j]	0.56[j]
V68N	1.2	0.0096	0.54	−0.02	−0.08	0.82[j]	0.78[j]

[a] 1eV=23.06 kcal mol^{-1} =96.5 kJ mol^{-1}

[b] Here the wild-type myoglobin is labeled as Mb, while the mutated myoglobins are labeled with the names of the mutants themselves such as H64I, H64L, or V68N

[c] Chelated protoheme mono-3-(1-imidazoyl)-propylamide monomethyl ester in benzene

[d] $\Delta E_{AB}=\Delta E_{bind}$(Mb-AB/mutant-AB) is the difference of the binding energies between wild-type Mb and the indicated mutant, estimated with the formula $\Delta E_{AB}=kT\Delta\ln k_{AB}$

[e] The ΔE_{AB} for the Mb is set to zero

[f] Dissociation barrier for Mb, corrected for the absence of the protein environment (ref. [52])

[g] Dissociation barrier for Mb (ref. [26])

[h] Estimated from i and relative CO/O_2 equilibrium constants (refs. [34, 51, 52])

[i] Dissociation barrier for chelated protoheme in benzene (ref. [51])

[j] Here E_{bind}(AB) [i.e., E_{bind}(Por-AB) or E_{bind}(Mb-AB), etc.]=E_{bind}(Mb-AB) − ΔE_{AB}

Por pure porphyrin.
Mb wild-type myoglobin.
H64I (histidine-64→isoleucine) mutated myoglobin.
H64L (histidine-64→leucine) mutated myoglobin.
V68N (valine-68→asparagine) mutated myoglobin.

The equilibrium constant K_{AB} (capital K), associated with both ligand association and dissociation rate constants (k'_{AB}, k_{AB}) ($K_{AB} = k'_{AB}/k_{AB}$), is related to ligand affinity. The dissociation rate constant k_{AB} is usually related to the active site-ligand binding (whereas k'_{AB} is related to ligand accessibility). Thus, the K_{CO}/K_{O2} value, also called M value, reflects the ratio of the CO and O_2 binding affinities to the given compound. It is 22000 when the compound is chelated protoheme in benzene, whereas that for Mb is 25 [34]. This difference in the M value (22000 vs. 25) is estimated to correspond to a discrimination energy of ca. 0.18 eV [27] (1 eV=23.06 kcal mol^{-1}= 96.5 kJ mol^{-1}), which is defined as

$$\begin{aligned}\Delta\Delta E &= \Delta[E_{bind}(Por-CO)-E_{bind}(Por-O_2)]-\Delta[E_{bind}(Mb-CO)-E_{bind}(Mb-O_2)]\\ &= \Delta[E_{bind}(Mb-O_2)-E_{bind}(Por-O_2)]-\Delta[E_{bind}(Mb-CO)-E_{bind}(Por-CO)].\end{aligned}$$

Three sets of experimental binding energies are given for CO/O_2 to a porphyrin. The first set (0.78 eV for CO and 0.53 eV for O_2) refers to the measured dissociation barriers for chelated protoheme dissolved in benzene [51]. The binding energies of the second set (0.79 eV for CO and 0.55 eV for O_2), which are given also for chelated protoheme in benzene, are estimated based on the measured dissociation rate constants k_{AB} and on the formula $\Delta E_{AB} = kT\Delta\ln k_{AB}$ [41]; they are shown to be very close to those of the first set. The third set refers to the dissociation barriers for Mb, corrected for the absence of the protein environment [52]; they should represent the binding energies of AB to a porphyrin in vacuum, and are seen to be notably different from those for chelated protoheme in benzene. Compared to the values for Por in vacuum, the binding energy of O_2 to Mb is increased by 0.26 eV, while the binding energy of CO to Mb is *reduced* by as much as 0.05 eV. Therefore, the discrimination energy between O_2 and CO by Mb should be as large as 0.31 eV, considerably higher than 0.18 eV that is usually cited in the literature [27]. The values for Por in benzene may not be best suited for comparison with computational results because they are not measured in the gas phase. It is known that the binding properties of AB to chelated protoheme can be different when the porphyrin is dissolved in different solvents [53].

On the theoretical side, Table 2 presents several calculations from the literature that included the protein environment. Blomberg et al. [26] considered an $FeP(NH_3)$(AB)···His64

model and calculated 0.70 and 0.78 eV for the Mb-CO and Mb-O_2 binding energies, respectively. The former is smaller than the latter, a trend which is opposite to the experimental one (0.80 eV for Mb-CO and 0.70 eV for Mb-O_2). Sigfridsson and Ryde [14, 15] applied a quantum mechanics/molecular mechanics (QM/MM) method to MbAB, treating heme(AB) plus His64 quantum mechanically and the proteins via molecular mechanics. Their calculated Mb-CO and Mb-O_2 binding energies are 1.08 and 1.00 eV, respectively; the relative energy of Mb-CO vs. Mb-O_2, Δ(Mb-CO/Mb-O_2), agrees with experiment (0.10 eV) well, though the absolute values are too large. These authors did not report binding energies of AB to a porphyrin, and so no comparison could be made between Mb-AB and Por-AB. Another QM/MM computation on MbAB was performed by Rovira et al. [25], but with His64 in the MM system. They calculated the H-bond strength between bound AB and His64 and obtained H-bond energies of 0.15 eV for CO and 0.22 eV for O_2; the value for CO is considerably too large and difference between the H-bond energies for O_2 and CO is too small (only 0.07 eV). These results may reflect limitations of the MM method in treating the effect of His64. On the other hand, all the calculated H-bond energies for bound CO···His64, which are always attractive, cannot account for the experimental trend that the heme-CO binding energy is decreased from Por to Mb.

Spiro and co-workers [27] carried out DFT computations on a large heme(AB) model system that includes the 13 closest, surrounding residues. They compared Mb to H64I, but just reported the relative energies between Mb-AB and H64I-AB (AB = CO, O_2); no information is provided about the absolute binding energies for Mb-AB and H64I-AB, nor is comparison made between Por-AB and Mb-AB.

After the above brief review of the experimental data and previous calculated results, we report, in the following, both our DFT and dispersion-corrected DFT calculations for the AB ligands on Por, Mb, H64L, and V68N. Recent calculations [54, 55] performed with the DFT + E_{disp} technique for weakly bound systems have been very promising; the new method is expected to yield improved quantitative results.

Computational details

Models

The system used for modeling the active site of Mb is illustrated in Fig. 2a. It is based on a high-resolution crystal structure of MbCO (pdb *code* 1BZR) [5]. Here the given closest residues surrounding the bound CO, above the porphyrin plane, are histidine-64 (His64), valine-68 (Val68), phenylalanine-43 (Phe43), isoleucine-107 (Ile107), leucine-29 (Leu29), and leucine-32 (Leu32), which have atoms falling within a ca. 8.0-Å radius of the Fe atom. Glycine-65 (Gly65) is covalently linked to His64. In our actual calculations, a somewhat simplified and protonated model is used, as shown in Fig. 2b. For example, the heme group is modeled as a porphine (P) without substituents and the proximal His93 is modeled as a 4-ethylimidazole (4-EtIm). It has been shown that FeP is able to mimic the essential properties of the more complicated FePPIX [21], and 4-EtIm is a well-simplified (both reliable and valid) model for the histidine residue attached to FePPIX [56]. The relatively distant (> 10 Å) Leu32, Gly65, Leu68, and His97 residues are excluded in the model. His64 is protonated at N_ε. A geometry optimization is then performed for the whole system.

Two optimization procedures are used: (1) Considering the fact that the residues around the heme(AB) are anchored to the polypeptide in the protein matrix, constraints are imposed on the residues in the geometry optimization; i.e., the terminal amino nitrogen atoms are fixed according to the crystal structure. (2) The distal residues above the heme plane are allowed to move freely in geometry optimizations. It would be of interest to give a comparison of the results of the two situations.

To model MbO_2, the crystal structure of MbCO is used, where CO is just replaced with O_2. In fact the crystal structure of *native* MbO_2 is also available (*code* 1A6M) [6], but does not show an obvious difference in the arrangements of the residues from that of MbCO. For comparison, we performed another set of calculations based on the crystal structure of *native* MbO_2. The results are presented in Table 3. It is shown that the calculated Mb-O_2 binding energies based on the two structures differ only slightly, which indicates that these interactions are almost equivalent.

The systems used for both H64L(CO) and H64L(O_2) are based on the crystal structure of H64L(CO) (*code* 2MGC) [57]. We chose H64L rather than H64I because the crystal structure of the CO complex of H64L is available, on which the calculations can be based directly. (H64I was used by Spiro and co-workers [27] in their calculations, where His64 in Mb was manually replaced by isoleucine.) However, no crystal structure is available for *native* H64L(O_2) to the best of our knowledge. We suppose here that the structure of the O_2 complex is also similar to that of the CO complex, with the exception of the Fe-O-O angle, which is ca. 120°.

In the case of V68N, both *native* crystal structures of the CO- and O_2 complexes (*code* 1M6C and 1MNO) [35] are available and have been used respectively as a starting point for modeling the active site of myoglobin. In contrast to MbCO, there are great changes in the distal heme pocket of V68N(CO) as a consequence of the V68N mutation. The distal His64 side chain in V68N(CO) has swung out of the pocket away from the CO ligand and toward the solvent (see Fig. 3c). However, such an upward movement of His64 in V68N(CO) does not occur in *native* V68N(O_2). The latter structure can apparently give a favorable H-bond interaction between bound O_2 and His64 (see Fig. 3d), but the former

Table 2 Calculated Mb-AB binding energies (E_{bind}, eV) and MbAB···His64 hydrogen-bond energies (E_{Hbond}, eV) from the literature

	Calcd (Exptl)[a]	Ref.	Model used
E_{bind}(Mb-CO)	0.70 (0.80)	[26]	FeP(NH_3)(AB) with one His64
E_{bind}(Mb-O_2)	0.78 (0.70)	[26]	
E_{bind}(Mb-CO)	1.08	[14, 15]	FeP(Im)(AB) with one His64 + surrounding point charges (QM/MM method)
E_{bind}(Mb-O_2)	1.00	[14, 15]	
E_{Hbond}(MbCO···His64)	0.08	[14, 15]	
E_{Hbond}(MbO_2···His64)	0.35	[14, 15]	
E_{Hbond}(MbCO···His64)	0.15	[25]	Heme(AB) with one His64 (QM/MM method)
E_{Hbond}(MbO_2···His64)	0.22	[25]	
ΔE_{bind}(Mb-CO/H64I-CO)[b]	0.04 (0.02)	[27]	Heme(AB) with 13 surrounding residues
ΔE_{bind}(Mb-O_2/H64I-O_2)[c]	0.18 (0.16)	[27]	

[a]The values in parentheses are experimental data from Table 1

[b]It is equal to ΔE_{CO} in Table 1

[c]It is equal to ΔE_{O2} in Table 1

structure does not. In Table 3, a comparison is also made between the calculated V68N-O_2 binding energies based on the two different crystal structures, and it is shown that E_{bind} in V68N(CO) is 0.1–0.2 eV smaller than that in V68N(O_2). Therefore, one must use the crystal structure of *native* V68N(O_2), rather than V68N(CO), to model V68N(O_2) in order to obtain "correct" results.

DFT and dispersion-corrected DFT methods

All calculations used the Amsterdam Density Functional (ADF) program package - ADF2012.01 [58, 59]. Three density functionals were used in the calculations. They are BP (which contains Becke's 1988 gradient correction for exchange [60] plus Perdew's 1986 gradient correction for correlation [61]), revPBE (revised Perdew-Burke-Ernzerhof functional [62] proposed in 1998 by Zhang and Yang [63]), and B3LYP (Becke's 1993 three-parameter hybrid functional [64] using the Lee-Yang-Parr correlation functional [65]). The heme-AB binding energies prove to be difficult to predict theoretically. We recently tested a large number of density functionals on the FeP(Im)(AB) systems (Im = imidazole; AB = CO, NO, O_2) and found that relatively satisfactory results for the various FeP(Im)-AB binding energies were obtained with the meta-GGA functionals BLAP3 and Bmτ1 [66]. But in the ADF program, these functionals are treated in a non-self-consistent (non-SCF) manner and so they are not suited for the present calculations on the rather large systems here (because a very high level of numerical-integration accuracy needs to be set in the non-SCF calculations of binding energies [66] and this is computationally too expensive for large systems). Among the various functionals tested, B3LYP and revPBE provided excellent binding energies for the AB = CO and O_2 ligands, respectively (B3LYP for CO and revPBE for O_2), and so they are adopted here.

The interaction between the bound AB and the surrounding residues in myoglobins is noncovalent (mainly hydrogen bonds and van der Waals forces here). As pointed out in the Introduction, the present-day density functionals cannot properly describe long-range electron correlations that are responsible for van der Waals dispersive forces. To account for dispersion in DFT, several approaches have been suggested and implemented [46]. One strategy is to add a (semi-)empirical correction of the form C_6R^{-6} to a density functional scheme to yield a DFT + E_{disp} model (it is denoted as DFT-D by some other authors [45]), in which the dispersion energy is calculated separately from the DFT calculations and simply added to the DFT energy [45]:

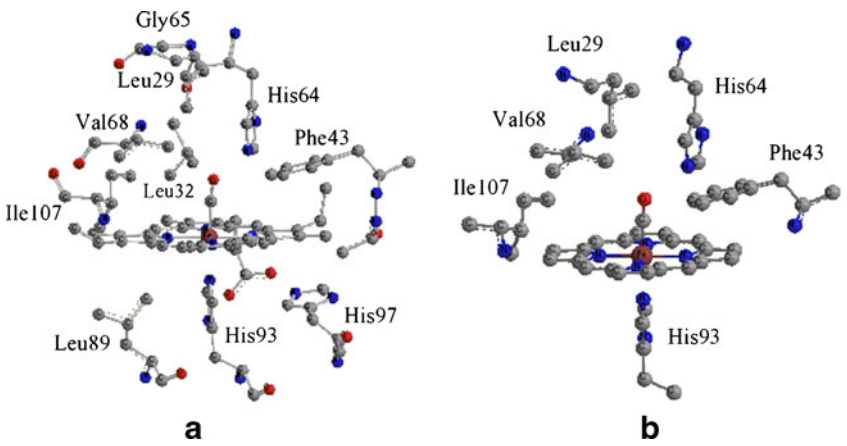

Fig. 2 **a** The structure and residues surrounding the bound CO in the wild-type MbCO (*code* 1BZR) (hydrogen atoms are omitted for clarity). **b** Model used in the calculations

Table 3 Comparison of the calculated Mb-O_2 binding energies (E_{bind}, eV) based on the crystal structures of the MbCO and MbO_2 proteins (i.e., in MbCO and MbO_2)[a]

[a]No constraints on the residues are imposed in the geometry optimization

	BP		PBE		revPBE	
	DFT	DFT-D1	DFT	DFT-D1	DFT	DFT-D1
In MbCO (*code* 1BZR)	0.96	0.89	1.05	0.98	0.66	0.65
In MbO_2 (*code* 1A6M)	0.94	0.86	1.10	1.02	0.63	0.65
in V68N(CO) (*code* 1M6C)	0.87	0.86	0.97	0.97	0.58	0.57
in V68N(O_2) (*code* 1MNO)	0.99	0.96	1.15	1.11	0.65	0.68

$$E_{\text{tot}} = E_{\text{DFT}} + E_{\text{disp}} \quad (1)$$

Here E_{disp} is described by a sum of damped interatomic potentials of the form C_6R^{-6}:

$$E_{disp} = -\sum_{n}\sum_{i<j} s_n \frac{C_n^{ij}}{R_{ij}^n} f_{d,n}(R_{ij}), \quad n = 6, 8 \quad (2)$$

where s_n is a global scaling factor, C_n^{ij} is the dispersion coefficient for atom pair ij and calculated from individual atomic C_n^i and C_n^j coefficients through a combination rule [48], and R_{ij} stands for an interatomic distance. The term $f_{d,n}(R_{ij})$ is a damping function, which is used to damp the R^{-n} term at short distances and to reduce the correlation effect on covalent bonds. The damping functional is fitted to each specific density functional.

Three versions of Grimme's dispersion correction have been implemented in ADF; they are labeled [48] as DFT-D1, -D2, and -D3, respectively. The

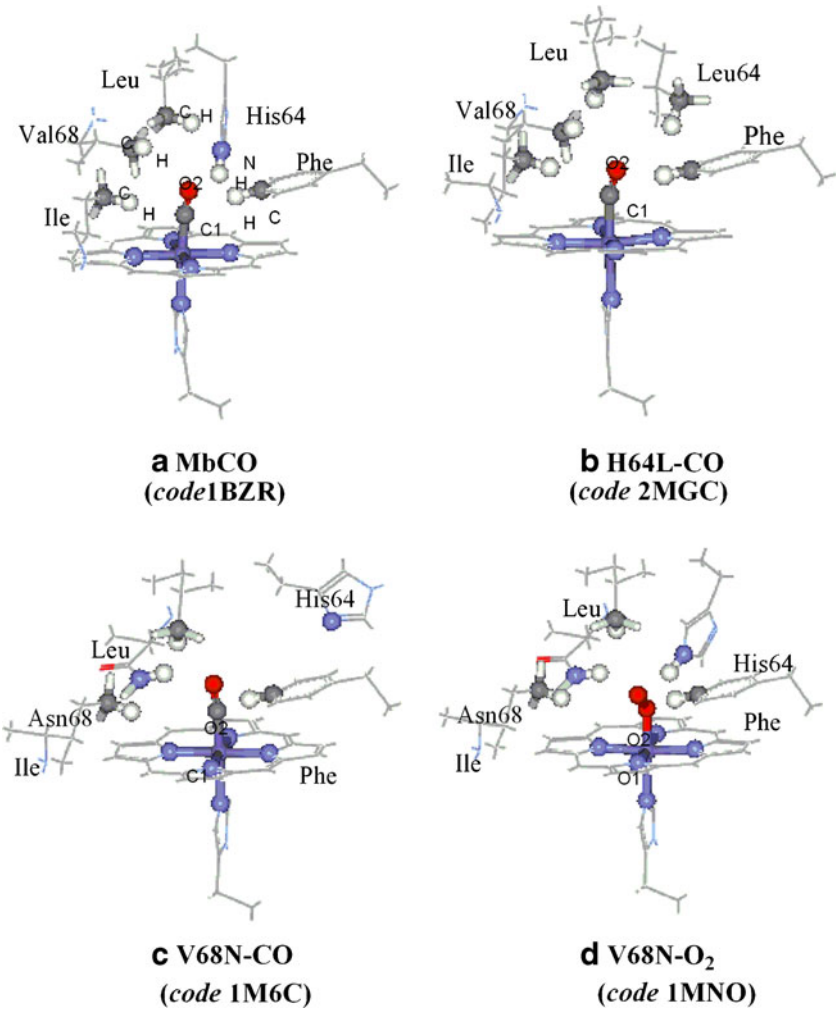

Fig. 3 The structures of various myoglobins showing the closest neighboring C (or N) and H atoms from the surrounding residues to the Fe-A-B moiety

damping functions in the different versions are given in Supplementary material.

More recently, a revised version of DFT-D3 was reported by Grimme et al. [49]. It uses the rational damping proposed by Becke and Johnson [67] (see Supplementary material). The variant that uses Becke and Johnson's damping, labeled as -D3(BJ), has been implemented in the updated ADF program (ADF2012.01). The current ADF also includes the density-dependent dispersion correction (dDsC) method developed by Steinmann and Corminboeuf [50, 68] (Supplementary material).

The relatively early -D1 version [45] was designed mainly for noncovalent interactions between molecules, assuming that within a covalent molecule, the effects of correlation are covered well by the particular exchange-correlation (XC) functional (although it may be argued that in the DFT + E_{disp} approach, the dispersion part is damped away at shorter distances and should not affect these). This version has been shown to give good results [45, 47, 55]. -D2 [54] is a slightly modified version of -D1, following a strategy in which the DFT description is restricted to shorter electron correlation ranges and to describe the medium to larger ranges by damped C_6R^{-6} terms. Thus, this newer version can be used for normal molecules. However, DFT-D2 has the tendency of overbinding at shorter intermolecular distances, probably because of a double-counting of correlation effects [69]. The -D3 version was developed recently [48] and contains many modifications and new features. In this work, the -D1, -D3, -D3(BJ), and -dDsC dispersion correction methods have been used.

The Slater-type orbital (STO) basis set used is the standard ADF-TZP, which is a triple-ζ plus one polarization function set. Frozen-core techniques [58] were used here to reduce the computational cost. To obtain accurate results, the valence set on Fe included subvalence 3s and 3p shells. For C, N, and O, 2s and 2p were considered as valence shells. The other shells of lower energy, i.e., [Ne] for Fe and [He] for C/N/O, were described as core and kept frozen. By using the large TZP basis sets, the basis set superposition error (BSSE) was found to be small and could be negligible[1].

Relativistic corrections for the valence electrons were calculated by the quasi-relativistic (QR) method [70]. For the open-shell states, the unrestricted Kohn-Sham (KS) spin-density functional approach was adopted.

[1] In fact, we do not need to consider BSSE in the present calculations at all because we do not calculate intermolecular binding energies in this work.

Results and discussion

Structure

We first discuss the molecular structures of FeP(4-EtIm)(AB) and the various model myoglobins [MbAB, H64L(AB), V68N(AB)], which are optimized with DFT and the various DFT + E_{dsip} methods. The DFT functional used is BP, which was shown to give an excellent description of molecular structure in previous calculations [56]. On the other hand, the changes in the calculated structure by using different functionals are insignificant in most cases [56]; in particular these changes do not lead to notable errors in the calculated energies. To further support this argument, Table 4 presents the calculated FeP(4-EtIm) − AB binding energies (E_{bind}) at the BP optimized structure and at the structure optimized with the respective individual functional itself. It is shown that the E_{bind} values obtained at the different functionals' optimized structures are nearly the same, the difference being at most 0.02 eV.

The calculated structural parameters of interest are all provided in Supplementary material, together with available experimental (X-ray) crystal structural data. Since the deoxy forms of myoglobin are relevant to the myoglobin-AB binding energies (see Binding energies of AB to porphyrin and the various myoglobins section), the Supplementary material also presents the calculated structural parameters of FeP(4-EtIm) without the AB ligand.

The d^6 Fe^{II} iron in deoxyHeme can exhibit three spin states, namely S=0 (low spin, singlet), S=1 (intermediate spin, triplet), and S=2 (high spin, quintet). The geometry optimization was performed for each spin state. Three critical coordination parameters of deoxyHeme are $R_{Ct(4N)\cdots N(eq)}$ (distance between the center of the porphyrin ring and the equatorial, porphinato nitrogen), $R_{Ct(4N)\cdots Fe}$ (distance between the center of the porphyrin ring and Fe), and $R_{Fe\text{-}N(ax)}$ (axial Fe-imidazole bond length). $R_{Ct(4N)\cdots N(eq)}$ is a measure of the porphinato core size and $R_{Ct(4N)\cdots Fe}$ represents the displacement of Fe out of the 4N-plane toward the axial imidazole ligand. Binding an AB ligand to the five-coordinate complex moves the Fe back into the plane. But $R_{Ct(4N)\cdots Fe}$ in heme(AB), though small, is not zero experimentally and may be different in different compounds [71]. Hence, we have also presented the calculated $R_{Ct(4N)\cdots Fe}$ values for each heme(AB). The other structural parameters of interest for a heme(AB) moiety include $R_{Fe\text{-}AB}$ (the axial Fe-AB bond length), $R_{A\text{-}B}$ (the A-B bond length), and $\angle_{FeAB}$ (the Fe-A-B bond angle). Heme(CO) has a closed-shell singlet ground state; the strong field of the CO ligand makes the six-coordinate system low spin. In the case of AB=O_2, the ligand field is relatively weak. There is an electron transfer from Fe to O_2, yielding an $Fe^{III} - O_2^-$ unit in the complex. Therefore, the ground state of heme(O_2) is either a triplet (S=1) $(d_{xy})^2(d_{xz})^2(d_{yz}\alpha)^1(O_2\text{-}\pi_g^*\alpha)^1$ or an open-shell singlet (S=0) $(d_{xy})^2(d_{xz})^2(d_{yz}\alpha)^1(O_2\text{-}\pi_g^*\beta)^1$. According to our

Table 4 Calculated FeP(4-EtIm) − AB binding energies (E_{bind}) at the BP optimized structure and at the structure optimized with the respective individual functional itself

		E_{bind}[FeP(4-EtIm) − AB], eV				
		BP	PBE	revPBE	RPBE	B3LYP
AB = CO	BP-struct[a]	1.56	1.66	1.31	1.25	0.81
	Indiv-struct[b]		1.66	1.31	1.25	0.79
AB = O_2	BP-struct	0.71	0.81	0.44	0.41	0.04
	Indiv-struct		0.80	0.45	0.42	0.03

[a] At the BP optimized structure.

[b] At the structure optimized with the respective individual functional itself

calculations, the triplet is somewhat lower in energy than the open-shell singlet for this complex. The ground state of FeP(L)(O_2) is shown to be different with different L [56]; a weaker Fe-L bond more likely leads to an open-shell singlet ground state for the oxy complex.

For the external structure of heme in a myoglobin, we give the distances between each of the Fe-A-B atoms and their nearest neighboring C (or N) and H atoms from each residue. These atoms are shown in Fig. 3 and indicated with big balls.

FeP(4-EtIm) and FeP(4-EtIm)(AB)

The calculated structural parameters of deoxyHeme can be rather different for different spin states. From Table S1 (Supplementary material), we see that $R_{Ct(4N)\cdots N(eq)}$ (core size) and $R_{Ct(4N)\cdots Fe}$ (Fe out-of-plane displacement) for S=2 are significantly larger than those in the lower-spin states. The experimental data used to compare with FeP(4-EtIm) are those measured for deoxyMb, which is high spin. We should point out here that the X-ray crystal structural data for the five-coordinate, synthetic FeTPP(2-MeIm) and FeTpivPP(2-MeIm) compounds are available in the literature [71]. 4-EtIm is similar to 1-MeIm, but rather different from 2-MeIm; see ref. [56] for more details. Concerning FeP(4-EtIm)(AB) (Table S2), we have X-ray structural data on comparable, synthetic FePor(L)(AB) compounds (here Por = TPP or TpivPP) [71].

For both FeP(4-EtIm) and FeP(4-EtIm)(AB), there is good quantitative agreement between the pure DFT calculations and experimental structures. The dispersion correction results in a shortening of the bonds between Fe and surrounding atoms; the axial Fe-N(ax) distance is decreased by 0.03–0.05 Å. But the other bonds Fe-N(eq) and Fe-AB are shortened only slightly by the dispersion correction. There are no notable differences among the DFT-D3, -D3(BJ), and -dDsC optimized structural parameters.

According to the $R_{Ct(4N)\cdots Fe}$ values, there is a notable out-of-plane displacement of Fe even in the six-coordinate system for AB = CO, where $R_{Ct(4N)\cdots Fe}$ amounts to −0.03 to −0.04 Å. The negative value just denotes that Fe is displaced toward the AB ligand. Fe in FeP(4-EtIm)(O_2) can be thought to lie in the porphyrin 4N plane because $R_{Ct(4N)\cdots Fe}$ in this complex is about −0.01 Å. The trend in $R_{Ct(4N)\cdots Fe}$ from AB = CO to AB = O_2 is consistent with the order of the binding strengths of the AB ligands to Fe (see Binding energies of AB to porphyrin and the various myoglobins section).

Except for $\angle_{FeAB}$, the experimental structural parameters of FePor(L)(AB) are in general quite close to those measured for MbAB. The Fe-A-B bond angle is shown to be smaller in MbAB than in FePor(L)(AB), which can be attributed to the interaction of bound AB with the protein environment in MbAB.

MbAB

From Por(AB) to MbAB, all the calculated R values undergo little changes. But the situation for $\angle_{FeCO}$ is different. The calculated Fe-C-O angles in MbCO vary from 174° to 179°, depending on the method used. The experimental Fe-C-O angle in the high-resolution MbCO crystal structure (*code* 1BZR) from ref. [5] is 171°, comparable to the DFT and DFT-D1 calculations without constraints on the residues in geometry optimization. The corresponding change in the calculated Fe-O-O angles is less pronounced; they vary from 129° to 131° and are about 3–5° smaller than those calculated in the pure porphyrin (~134°). The crystal structural data of MbO_2 (*code* 1A6M) from ref. [6] are probably less accurate, which give a significantly smaller Fe-O-O angle (123°) than the calculations. Within the internal structure of heme, the DFT and DFT + E_{disp} optimized parameters are quite similar. That is, the dispersion effects between the heme and the protein environment do not notably affect the internal structure of the heme.

However, the external structure of heme in the myoglobin can be changed very much by dispersion effects. Owing to the attractive property of the dispersion interaction, the DFT + E_{disp} calculations give, in most cases, considerably shorter distances between the FeAB atoms and the protein residues than the DFT ones. As expected, the calculations with pure DFT greatly overestimate the intermolecular distances in MbAB, even when the terminal amino nitrogen atoms are frozen in the geometry optimization. Examining the tables in Supplementary material, we see that the distances optimized with DFT-D1 compare in most cases favorably with the X-ray crystal structural data for each of the MbAB, H64L(AB), and V68(AB) systems. With the DFT-D1 method, moreover, the geometry optimizations with and without constraints on the residues give similar structures, indicating that the modeled heme site is quantum mechanically stable. In a few cases for MbO_2, H64L(CO), or V68N(AB), the DFT-D1 optimized distances are still significantly larger than the experimental ones, even when dispersion

corrections are taken into account. It should be pointed out that the crystal structural data of a myoglobin measured with relatively low resolution may not be accurate enough. For example, the experimental Fe-C-O angle of 156° for the H64L(CO) structure (*code* 2MGC) cannot be considered to be correct (see next subsection). Various factors may influence the accuracy of the crystal structural data of a myoglobin[2]. Nevertheless, we see that the experimental distances for MbCO measured with high resolution (*code* 1BZR) are very well reproduced by the calculations with DFT-D1.

On going from DFT-D1 to DFT-D3, the optimized intermolecular distances are further shortened and they are now too short for Phe43, Ile10, and Leu29 as compared to experiment. The optimization with constraints on the residues (i.e., constrained optimization) improves the results in some cases. DFT-D3(BJ) gives much longer distances than DFT-D3 for Leu29 and so improves the agreement between the calculation and experiment, but this is true only when the constrained optimization is performed. With the constraints on the residues, the DFT-dDsC optimized structural parameters are comparable to those obtained with DFT-D3(BJ). Without constraints, DFT-dDsC appears to yield better results than DFT-D3(BJ) or DFT-D3 for the structure.

The structure of the Mb moiety in MbAB is changed notably when CO is replaced with O_2. The distal His64 group in MbO_2 comes so close to the O_2 molecule that it can form a fairly strong H-bond to the oxygen bound to Fe. This leads to an elongation of the other Fe···residue distances in MbO_2.

H64L(AB)

In this mutant, the Fe-C-O bond angles calculated with every method are all about 178°; their deviation from linearity is only ca. 2°. This appears to be smaller than that in MbCO (~6°). Nevertheless, the internal structure of the heme changes little from MbCO to H64L(CO) according to the calculations. The same is true for AB = O_2. But there are some differences in the positions of the residues between the MbCO and H64L(CO) structures; the Fe···residue distances are usually shorter in the former than in the latter. However, there are no significant differences in the Fe···residue distances between MbO_2 and H64L(O_2) according to the calculations.

When the optimized structure of H64L(CO) is compared to the X-ray crystal structure of the mutant, large differences can be seen. The measured Fe-C-O angle is very bent (156°) and there is a large out-of-plane displacement of Fe toward the axial His93 ligand. The other measured R values within the heme are also significantly larger than the calculated ones, and they indicate that heme(CO) has some character of deoxyHeme. The X-ray crystal structural data for H64L(CO) cannot be considered to be reliable. No *native* crystal structure is available for H64L(O_2).

V68N(AB)

When Val68 in Mb is replaced with Asn, the linearity of the FeCO unit is restored. Val68 in MbCO is in close van der Waals contact with the bound ligand and has been suggested to be responsible for the small distortion of Fe-C-O from linearity [27]. Certain calculations support this argument. We note in the above section that the bending of Fe-C-O is smaller in H64L(CO) than in MbCO. This is because the His64→Leu substitution makes Val68 shift away from the heme center; theVal68 carbon atom in H64L(CO) is at longer distance from the bound ligand than in MbCO. As a result, the steric hindrance from Val68 to the bound CO is weakened from MbCO to H64L(CO).

The V68N mutation involves the substitution of the isopropyl side chain of Val68 by the acetamide side chain of Asn, a replacement which is expected to alter the polarity of the distal heme pocket in myoglobin. The orientation of the Asn68 side chain is well defined with its -NH_2 group toward the bound CO; such an orientation is expected to favor oxygen binding by providing an additional H-bond to the highly polar Fe-O_2 complex.

A notable feature of the V68N(CO) crystal structure is that the distal His64 side chain has swung out of the pocket away from the CO ligand (see Fig. 3c). However, such an upward movement of His64 does not occur in the structure of *native* V68N(O_2) (Fig. 3d). But one part of the experimental V68N(O_2) structure appears to be unusual: Fe is displaced greatly to the proximal side; the Ct(4N)···Fe distance is as large as 0.13 Å. According to the calculations, however, the Fe atom is almost in the heme plane for the six-coordinate O_2 complex, there being no difference from the position in MbO_2 and H64L(O_2).

Binding energies of AB to porphyrin and the various myoglobins

We now turn to our discussion on the binding energies of the AB ligands to the porphyrin (Por) [i.e., FeP(4-EtIm)] and to the various myoglobins (Mb, H64L, V68N). E_{bind}(Por-AB) is defined as

$$-\mathrm{E_{bind}(Por-AB)} = E[\mathrm{Por(AB)}] - \{\mathrm{E(Por)} + \mathrm{E(AB)}\}.$$

In the case of a myoglobin, e.g., MbAB, E_{bind} is defined as

$$-\mathrm{E_{bind}(Mb-AB)} = E(\mathrm{MbAB}) - \{E(\mathrm{deoxyMb}) + E(\mathrm{AB})\}.$$

Here E[Por(AB)], E(Por), E(MbAB), E(deoxyMb), and E(AB) are total energies of the indicated species, which are optimized independently. The ground states of FeP(4-EtIm) and deoxyMb can be different when different functionals are

[2] The crystal coordinates are not the experimental raw data; they are a product of an involved series of model building, crystallographic refinement, manual examination, and rebuilding, possibly involving mistakes in interpretation.

used. Table 5 presents the calculated relative energies ($E^{relative}$) for selected states (S=0, 1 2) of the two systems with the several functionals adopted here. BP predicts a singlet ground state for FeP(4-EtIm), while a triplet ground state is predicted by revPBE. Finally, B3LYP gives the correct (experimental) ground state multiplicity for this system. A comparison between our B3LYP results and those from the literature is given in Supplementary material (Table S9); they agree well with each other. The protein environment as well as the dispersion correction is shown to have little effect on the spin-state energetics of deoxyHeme. The calculated E_{bind} refers to the species in the calculated ground state. Several reports [20, 26, 30, 32, 52] have been published on the BP and B3LYP calculated FeP(Im)-AB binding energies (AB = CO, O_2). They are comparable to our E_{bind} results (Supplementary material, Table S10). Some differences in the calculated results with the same functional arise mainly from the different basis sets employed [66]. The calculated E_{bind} results from some references [32, 52] include a correction (Δ_{ZPVE}) for zero-point vibrational energy (ZPVE). According to our previous calculations [66] and others [52], the Δ_{ZPVE} contribution to E_{bind} is about 0.1 eV. Our E_{bind} results presented here do not include Δ_{ZPVE}.

The DFT and DFT-D1 calculated results are collected in Table 6, together with available experimental data for comparison. It is shown that the calculated E_{bind} is rather sensitive to the choice of functional. We have thus presented the relative binding energies between myoglobin-AB and Por-AB, ΔE_{bind}(myoglobin-AB/Por-AB). These are given in Table 7. Owing to error cancellation, ΔE_{bind} is much less dependent on the specific functional and should be more useful to assess the performance of the dispersion correction in the DFT calculations. Table 8 presents some other calculated relative binding energies and the evaluated discrimination energies.

A comparison of the calculated energies (E_{bind}, ΔE_{bind}) with DFT and the various DFT + E_{disp} methods (−D1, -D3, -D3(BJ), -dDsC) are reported in Supplementary material. -D3(BJ) and -dDSc have only been tested on Por(AB) and MbAB (AB = CO, O_2). We have shown in Structure section that the DFT-D3 approach gives too short distances between the residues and the heme moiety in the myoglobins. This may imply that the dispersion energies in these large biological molecules are probably significantly overestimated by DFT-D3. As a result, its calculated relative energies are in poor agreement with experiment in most cases. Some improvements of the results are obtained with DFT-D3(BJ) when constraints on the residues are imposed in the geometry optimization. With this optimization procedure, DFT-dDSc gives better results than DFT-D3(BJ) for ΔE_{bind}(Mb-O_2/Por-O_2), but provides poorer results for ΔE_{bind}(Mb-CO/Por-CO). Without constraints on the residues in the geometry optimization, the DFT-dDsC approach is shown to yield very poor results for both ΔE_{bind}(Mb-O_2/Por-O_2) and ΔE_{bind}(Mb-CO/Por-CO).

In contrast, the DFT-D1 approach yields the model structures which agree very well with the X-ray crystal structural determinations in high resolution, and its geometry optimizations with and without constraints on the residues give similar structures. As a results, the DFT-D1 calculated energies with the different optimization procedures are similar as well and agree well with the experimental ΔE_{bind} data. In the following, the effects of the local protein environment are discussed mainly based on the results obtained with DFT-D1 and with the constrained optimization, unless otherwise stated.

Por-AB

For comparison, Por-AB is also of interest as it is the reference point for discussing the effects of the local protein environment on the heme-AB binding. The calculated binding energies E_{bind}(Por-AB) with the BP functional are 1.56 and 0.71 eV for AB = CO and O_2, respectively[3]. They are larger than the experimental data (CO: 0.85 eV, O_2: 0.44 eV) by 0.71 and 0.27 eV, respectively for the two ligands. The revPBE functional performs much better than BP and gives E_{bind}(Por-O_2) which is in excellent agreement with experiment. Nevertheless, this functional still overestimates E_{bind}(Por-CO) by 0.46 eV. While the pure GGA functionals seriously overbind for AB = CO, the hybrid functional B3LYP clearly provides a superior result for this ligand (0.81 eV). But it gives too small a binding energy for AB = O_2 (0.04 eV).

When the dispersion correction is made, the binding energies obtained with DFT-D3 increase by ca. 0.14, 0.24, and 0.26 eV for the BP, revPBE, and B3LYP functionals, respectively (see Supplementary material). The dispersion contributions to E_{bind} are similar for AB = CO and O_2. Since BP and revPBE already give too large a binding energy for Por-CO and revPBE works very well for Por-O_2, the addition of the dispersion term causes the performance of the two functionals to deteriorate. The DFT-D3(BJ) method gives similar results to those of DFT-D3 for AB = CO; but there is a reduction of 0.05–0.1 eV in the calculated E_{bind}(Por-O_2) on going from -D3 to -D3(BJ). Some increase, ranging from 0.02 to 0.16 eV depending on functional, in the DFT-dDsC calculated E_{bind}(Por-AB) is obtained as compared to DFT-D3.

[3] Previous calculations with all-electron method (ref. [56]) or with an increased accuracy of the numerical integration (ref. [66]) could give FeP(4-EtIm)-AB binding energies which are somewhat larger than the present ones. Owing to error cancellations, the present calculated results are actually in closer agreement with experiment than the previous ones.

Table 5 Calculated relative energies ($E^{relative}$, eV) for selcted states of FeP(4-EtIm) and deoxyMb

	FeP(4-EtIm)			deoxyMb (DFT)			deoxyMb (DFT-D1)		
	S=1	S=0	S=2	S=1	S=0	S=2	S=1	S=0	S=2
BP	0	−0.02	0.48	0	−0.01	0.50	0	−0.04	0.48
PBE	0	−0.03	0.46	0	0.02	0.45	0	−0.02	0.45
RPBE	0	0.12	0.29	0	0.16	0.28	0	0.16	0.29
revPBE	0	0.09	0.33	0	0.13	0.34	0	0.12	0.33
B3LYP	0	0.41	−0.09	0	0.44	−0.08	0	0.42	−0.09

For the B3LYP functional, the dispersion term greatly improves the result for E_{bind}(Por-O_2). The repulsive behavior of B3LYP for Por-O_2 seems to indicate inadequate treatment of dispersion effects in DFT, but the dispersion correction shows deficiency when this functional is applied to Por(CO). It would be wrong to assume that the interaction energy obtained with these functionals is dispersion-free; some form of compensation for the missing component (dispersion) of the interaction energy must exist.

Mb-AB

We now put heme(AB) in Mb and examine the influence of the local protein environment on the heme-AB binding. First

Table 6 Calculated binding energies (E_{bind}, eV)[a] of CO and O_2 to pure porphyrin (Por) [i.e., FeP(4-EtIm)] and to the models of wild-type Mb and two mutants (H64L, V68N) of myoglobin with DFT and DFT-D1

		BP	revPBE	B3LYP	Exptl
Por-CO	DFT	1.56	1.31	0.81	0.85[b] (0.78)[c]
Por-O_2	DFT	0.71	0.44	0.04	0.44[b] (0.53)[d]
Mb-CO	DFT	1.52 (1.45)	1.25 (1.16)	0.77 (0.70)	0.80[e]
	DFT-D1	1.52 (1.50)	1.32 (1.30)	0.76 (0.75)	
Mb-O_2	DFT	0.91 (0.96)	0.61 (0.66)	0.28 (0.35)	0.70[e]
	DFT-D1	0.87 (0.89)	0.64 (0.65)	0.28 (0.31)	
$Mb^{only\ His64}$-CO	DFT	1.59 (1.57)	1.35 (1.32)	0.83 (0.80)	
	DFT-D1	1.60 (1.55)	1.36 (1.30)	0.84 (0.80)	
$Mb^{only\ His64}$-O_2	DFT	0.94 (0.92)	0.65 (0.61)	0.31 (0.27)	
	DFT-D1	0.88 (0.86)	0.61 (0.59)	0.27 (0.24)	
$Mb^{no\ His64}$-CO	DFT	1.54 (1.55)	1.32 (1.33)	0.82 (0.84)	
	DFT-D1	1.56 (1.55)	1.34 (1.33)	0.79 (0.78)	
$Mb^{no\ His64}$-O_2	DFT	0.73 (0.77)	0.49 (0.52)	0.13 (0.16)	
	DFT-D1	0.75 (0.71)	0.53 (0.50)	0.12 (0.09)	
H64L-CO	DFT	1.51 (1.51)	1.29 (1.26)	0.81 (0.82)	0.79[f]
	DFT-D1	1.50 (1.48)	1.36 (1.34)	0.77 (0.74)	
H64L-O_2	DFT	0.73 (0.76)	0.49 (0.49)	0.17 (0.19)	0.56[f]
	DFT-D1	0.78 (0.73)	0.58 (0.52)	0.18 (0.13)	
V68N-CO	DFT	1.56 (1.58)	1.32 (1.32)	0.81 (0.84)	0.82[f]
	DFT-D1	1.62 (1.61)	1.36 (1.37)	0.83 (0.81)	
V68N-O_2	DFT	0.99 (0.99)	0.64 (0.65)	0.39 (0.44)	0.78[f]
	DFT-D1	1.00 (0.96)	0.72 (0.68)	0.45 (0.42)	

[a] The calculated results *not* in parentheses are those for the systems where the terminal amino nitrogen atoms are fixed according to the crystal structure in the geometry optimization; the calculated results in parentheses are those for the systems where the distal residues above the heme plane are allowed to move freely in the geometry optimization; the same is true for Tables 7 and 8

[b] Dissociation barrier for Mb, corrected for the absence of the protein environment (ref. [52])

[c] Estimated from *c* and relative CO/O_2 equilibrium constants (refs. [34, 51, 52])

[d] Dissociation barrier for chelated protoheme in benzene (ref. [51])

[e] Dissociation barrier for Mb (ref. [26])

[f] See Table 1

looking at the results obtained with pure DFT, the calculated Mb-CO binding energies are 1.52, 1.25, and 0.77 eV for the BP, revPBE, and B3LYP functionals, respectively; they are 0.04–0.06 eV smaller than those for Por-CO, the ΔE_{bind} values being close to the experimental one (−0.05 eV). Without constraints on the residues in geometry optimization, the relative binding energies between Mb-CO and Por-CO would be −0.11 to −0.15 eV; the constrained optimization improves the results of pure DFT. When a dispersion correction is made, there are little changes in E_{bind}(Mb-CO) for BP and B3LYP. But the DFT-D1 calculation with revPBE gives an Mb-CO binding energy which is similar to the Por-CO one. It is shown that the DFT-D1 calculated E_{bind}(Mb-CO) values with and without constraints on the residues in geometry optimization, are almost the same; the same is true for Mb-O_2. This is somewhat different from the case of pure DFT.

In contrast to the CO ligand, the bound O_2 is greatly stabilized by the protein environment. Depending on the functional used, the calculated Mb-O_2 binding energy is larger than the Por-O_2 one by 0.17–0.24 eV from the DFT calculations and by 0.16–0.24 eV from the DFT-D1 calculations. These values are comparable to the experimental one (0.26 eV). Similar ΔE_{bind}(Mb-O_2/Por-O_2) values are obtained with DFT-dDsC (0.15–0.20 eV). Without constraints on the residues in geometry optimization, the dispersion effects are found to destabilize the heme-O_2 binding. We should point out that the dispersion energy between any bound AB and the surrounding residues is always attractive, but according to the above definition for E_{bind}, the calculated Mb-AB binding energy is also related to the energy of *optimized* deoxyMb. The non-covalent interaction between the protein environment and the heme is enhanced when AB departs. Table 9 presents the estimated dispersion energies E_{disp} between the heme(AB) moiety and the considered surrounding residues in MbAB; they are 0.71 and 0.63 eV for AB = CO and O_2, respectively. Subtracting the E_{disp} portion between the AB ligand and residues, these values amount to 0.58 and 0.54 eV respectively. When AB departs, the structure of Mb is changed and the E_{disp} between the high-spin deoxyHeme and the surrounding residues in deoxyMb becomes 0.72 eV, which is larger than that (0.58 or 0.54 eV) in MbAB. The calculated E_{disp} in deoxyMb is insensitive to the spin state of deoxyHeme.

To examine the specific role of His64 in the distal pocket, additional calculations were also performed on a model system that includes only His64 (case 1) and on another model system that excludes it from the residues (case 2). In both cases, the DFT and DFT-D1 calculated Mb-CO binding energies are very similar and close to the Por-CO one. For AB = O_2, however, the two cases give rather different results. In case 1, the calculated Mb-O_2 binding energy is similar to that for the system that has all five residues; it is therefore significantly larger than the Por-O_2 one. In case 2, however, the exclusion of His64 in the system leads to a large (~0.15 eV) decrease in E_{bind} and the calculated Mb-O_2 binding energies are only slightly larger than the Por-O_2 ones. These results further support the previous conclusions [27] which show that His64 provides the dominant electrostatic stabilization for bound O_2 and the contributions of the other residues to the discrimination between O_2 and CO are small. The dispersion effects in case 1 are also found to destabilize the bound O_2. We note that the calculations on such a model do not give the experimental trend that the binding energy is lowered from Por-CO to Mb-CO; they give an opposite trend instead.

H64L-AB

According to the experimental data (Table 1), the heme-CO binding energy is slightly lowered by 0.01 eV when His64 in Mb is replaced with Leu. The DFT and DFT-D1 calculations with BP show that E_{bind}(H64L-CO) is 0.01–0.02 eV smaller than E_{bind}(Mb-CO) (see Table 8), in good agreement with the experiment value. The calculations with the other functionals yield slightly large binding energies for H64L-CO than for Mb-CO. Without constraints on the residues in geometry optimization, the ΔE_{bind}(Mb-CO/H64L-CO) values calculated with pure DFT are rather negative, in strong disagreement with experiment. However, the experiment-theory agreement is improved greatly by making a dispersion correction.

In the case of AB = O_2, the decrease in E_{bind} from Mb-AB to H64L-AB is significant, 0.14 eV according to experiment, 0.12–0.18 eV from the DFT calculations, and ~0.10 eV based on the DFT-D1 calculations. Somewhat large ΔE_{bind}(Mb-O_2/H64L-O_2) values are obtained without constraints on the residues in geometry optimization. The protein environment in H64L with His64 replaced by Leu has some stabilizing effect on the bound O_2. The experimental relative binding energy of H64L-O_2 vs. Por-O_2, ΔE_{bind}(H64L-O_2/Por-O_2), is as large as 0.12 eV, which is in good agreement with the DFT-D1 calculations (0.07–0.14 eV). We note that the calculated H64L-O_2 binding energies are not notably different from the $Mb^{no\ His64}$-O_2 ones.

V68N-AB

In contrast to H64L, the binding of AB to heme is enhanced by replacing Val68 in Mb with Asn, whose amide group has the capacity to serve as a H-bond donor (see V68N(AB) section and Fig. 3c or d). According to the calculations, the V68N-CO binding energy is 0.04–0.10 eV higher than the Mb-CO one, depending on the functional used. The experimental relative energy ΔE_{bind}(V68N-CO/Mb-CO) is 0.02 eV. The interaction between Asn and bound CO is

Table 7 Calculated relative binding energies (ΔE, eV) between myoglobin-AB and Por-AB, ΔE(myoglobin-AB/Por-AB)

		BP	revPBE	B3LYP	Exptl[b]
ΔE(Mb-CO/Por-CO)[a]	DFT	−0.04 (−0.11)	−0.06 (−0.15)	−0.04 (−0.11)	−0.05
	DFT-D1	−0.04 (−0.06)	0.01 (−0.01)	−0.05 (−0.06)	
ΔE(Mb-O_2/Por-O_2)[a]	DFT	0.20 (0.25)	0.17 (0.22)	0.24 (0.31)	0.26
	DFT-D1	0.16 (0.18)	0.20 (0.21)	0.24 (0.27)	
ΔE($Mb^{only\ His64}$-CO/Por-CO)	DFT	0.03 (0.01)	0.04 (0.01)	0.02 (−0.01)	
	DFT-D1	0.04 (−0.01)	0.05 (−0.01)	0.03 (−0.01)	
ΔE($Mb^{only\ His64}$-O_2/Por-O_2)	DFT	0.23 (0.21)	0.21 (0.17)	0.27 (0.23)	
	DFT-D1	0.17 (0.15)	0.17 (0.15)	0.23 (0.20)	
ΔE($Mb^{no\ His64}$-CO/Por-CO)	DFT	−0.02 (−0.01)	0.01 (0.02)	0.01 (0.03)	
	DFT-D1	0.00 (−0.01)	0.03 (0.02)	−0.02 (−0.03)	
ΔE($Mb^{no\ His64}$-O_2/Por-O_2)	DFT	0.02 (0.06)	0.05 (0.08)	0.09 (0.12)	
	DFT-D1	0.04 (0.00)	0.09 (0.06)	0.08 (0.05)	
ΔE(H64L-CO/Por-CO)	DFT	−0.05 (−0.05)	−0.02 (−0.05)	0.00 (0.01)	−0.06
	DFT-D1	−0.06 (−0.08)	0.05 (0.03)	−0.04 (−0.07)	
ΔE(H64L-O_2/Por-O_2)	DFT	0.02 (0.05)	0.05 (0.05)	0.13 (0.15)	0.12
	DFT-D1	0.07 (0.02)	0.14 (0.08)	0.14 (0.09)	
ΔE(V68N-CO/Por-CO)	DFT	0.00 (0.02)	0.01 (0.01)	0.00 (0.03)	−0.03
	DFT-D1	0.06 (0.05)	0.05 (0.06)	0.02 (0.00)	
ΔE(V68N-O_2/Por-O_2)	DFT	0.28 (0.28)	0.20 (0.21)	0.35 (0.40)	0.34
	DFT-D1	0.29 (0.25)	0.28 (0.24)	0.41 (0.38)	

[a] $\Delta E(\text{Mb-AB/Por-AB}) = E_{bind}(\text{Mb-AB}) - E_{bind}(\text{Por-AB})$; the same is true for other entries

[b] Based on the experimental data given in Table 6

somewhat overestimated by the calculations. Again, the constrained optimizations greatly improve the results of the pure-DFT calculations.

The binding energy of O_2 to heme is increased by 0.08 eV from Mb to V68N according to experiment. The DFT-D1 calculated relative binding energies ΔE_{bind}(V68N-O_2/Mb-O_2) are 0.08–0.17 eV, depending on the functional used; they are in reasonable agreement with experiment. The results of revPBE are improved significantly when a dispersion correction is made. On the other hand, the

Table 8 Some other calculated relative binding energies (ΔE, eV) and the evaluated discrimination energies (ΔΔE, eV)

		BP	revPBE	B3LYP	Exptl[c]
ΔE(Por-CO/Por-O_2)	DFT	0.85	0.87	0.77	0.41
ΔE(Mb-CO/Mb-O_2)	DFT	0.61 (0.49)	0.64 (0.50)	0.49 (0.35)	0.10
	DFT-D1	0.65 (0.61)	0.68 (0.65)	0.48 (0.44)	
ΔΔE (discrimination E)[a]	DFT	0.24 (0.36)	0.23 (0.37)	0.28 (0.42)	0.31
	DFT-D1	0.20 (0.24)	0.19 (0.22)	0.29 (0.33)	
ΔE(Mb-CO/H64L-CO)	DFT	0.01 (−0.06)	−0.04 (−0.10)	−0.04 (−0.12)	0.01
	DFT-D1	0.02 (0.02)	−0.04 (−0.04)	−0.01 (0.01)	
ΔE(Mb-O_2/H64L-O_2)	DFT	0.18 (0.20)	0.12 (0.17)	0.11 (0.16)	0.14
	DFT-D1	0.09 (0.16)	0.06 (0.13)	0.10 (0.18)	
ΔΔE (discrimination E)[b]	DFT	0.17 (0.26)	0.16 (0.27)	0.15 (0.28)	0.13
	DFT-D1	0.07 (0.14)	0.10 (0.17)	0.11 (0.17)	
ΔE(Mb-CO/V68N-CO)	DFT	−0.04 (−0.13)	−0.07 (−0.16)	−0.04 (−0.14)	−0.02
	DFT-D1	−0.10 (−0.11)	−0.04 (−0.07)	−0.07 (−0.06)	
ΔE(Mb-O_2/V68N-O_2)	DFT	−0.08 (−0.03)	−0.03 (0.01)	−0.11 (−0.09)	−0.08
	DFT-D1	−0.13 (−0.07)	−0.08 (−0.03)	−0.17 (−0.11)	

[a] ΔΔE (discrimination energy)=ΔE(Por-CO/Por-O_2)−ΔE(Mb-CO/Mb-O_2)

[b] $\Delta\Delta E = \Delta E(\text{Mb} - \text{O}_2/\text{H64L} - \text{O}_2) - \Delta E(\text{Mb} - \text{CO}/\text{H64L} - \text{CO}) = \Delta E(\text{H64L} - \text{CO}/\text{H64L} - \text{O}_2) - \Delta E(\text{Mb} - \text{CO}/\text{Mb} - \text{O}_2)$

[c] Based on the experimental data given in Table 6

Table 9 Calculated dispersion energies (in eV) between the heme(AB) moiety and the surrounding residues in AB-myoglobins, E_{disp}[heme(AB) − (residues)], and the dispersion energies between the deoxyHeme and the surrounding residues in deoxy-myoglobins, E_{disp}[deoxyHeme − (residues)]

	E_{disp}[heme(AB) − (residues)]		E_{disp}[deoxyHeme − (residues)]		
	AB = CO	AB = O_2	S=1	S=0	S=2
in Mb (*code* 1BZR)	0.71 (0.13)[a]	0.63 (0.09)[a]	0.71	0.72	0.72
in H64L (*code* 2MGC)	0.51 (0.07)	0.59 (0.06)	0.69	0.61	0.62
in V68N (*code* 1M6C)	0.56 (0.07)	[0.53 (0.06)][b]	0.51	0.52	0.54

[a] The values in parentheses are the E_{disp} portion between the AB ligand and the residues

[b] These values are 0.79 (0.11) eV when calculated based on the crystal structure of *native* V68N(O_2) with the *code* 1MNO

experimental relative binding energy of V68N-O_2 vs. Por-O_2 (0.34 eV) is well reproduced by the DFT-D1 calculations (0.28–0.41 eV).

Conclusions

The effects of local protein environment on the binding of diatomic molecules (CO, O_2) to heme in myoglobins have been studied in detail with both DFT and dispersion-corrected DFT methods. Several dispersion correction approaches, -D1, -D3, D3(BJ), and -dDsC, were tested in the calculations. In the -D1 approach, the dispersion correction (E_{disp}) is calculated only for noncovalent interactions between molecular fragments and E_{disp} within a covalent interaction is not calculated. It is shown that DFT-D1 performs very well, ensuring structural and energetic features in close agreement with experiment. Surprisingly, satisfactory energetic results are also obtained with the pure DFT method when constraints on the residues are imposed in the geometry optimization. This may be ascribed to error cancellations in the DFT calculated results.

By calculating and comparing the binding energies of O_2 and CO to a porphyrin and the various myoglobins, more details about the interaction between the protein environment and the bound ligand can be revealed. Based on the dissociation barriers for Mb, corrected for absence of the protein environment, the binding energy of O_2 to Mb is 0.26 eV (1 eV=23.06 kcal mol^{-1}=96.5 kJ mol^{-1}) increased as compared to that of a free porphyrin, while the binding energy of CO to Mb is reduced by 0.05 eV. The calculated results are in good agreement with both experimental data and the observed trend. Although the protein environment gives a favorable H-bond interaction for bound CO, it destabilizes the heme-CO binding. This is because the Mb-AB binding energy is also related to the energy of *optimized* deoxyMb, and the non-covalent interaction between the heme and the protein environment is enhanced when AB departs. Olson and Phillips [34] attributed most of this inhibition to the requirement of water displacement from the distal pocket. (The distal residues often bring a water molecule into the protein, which must be displaced before ligands can bind.) An alternative argument is that there exists repulsive interaction between the His64 side chain and the bound CO ligand [5]. The calculations show that this inhibition results from a change in the interaction between heme and residues with and without the AB ligand. In the case of O_2, the very strong H-bond interaction for this ligand over-compensates very much the mentioned enhanced, extra interaction. Therefore, we can still see a great stabilization of bound O_2 by the protein environment on going from Por to Mb.

The specific role of histidine-64 in the distal pocket has been examined in more detail in this study than in other studies in the literature. According to the calculations, the stabilization of heme-O_2 in Mb by a single His64 is ca. 0.20 eV, whereas the sum of the energetic contributions from the other residues to the heme-O_2 binding is about 0.05 eV. The small distortion of the Fe-C-O moiety from linearity in the high-resolution crystal structure of MbCO [5] is due to the steric hindrance from Val68 to the bound CO. This is consistent with previous calculated results of Spiro and co-workers [27]. The changes in the experimental binding energies from Mb-AB to H64L-AB or to V68N are also well reproduced by the calculations.

The performances of the advanced -D3, -D3(BJ), as well as -dDsC dispersion correction methods appear to be questionable for large biological molecules. These methods take into account intramolecular dispersion contribution for a covalent molecule. There are, however, some disputes as to whether this is desirable [46], since various approximate DFT methods that include GGA or hybrid GGA have been remarkably successful in describing a wide variety of strongly interacting systems. This may imply that the contribution of the dispersion energy, which is missing from the DFT treatment, is compensated for to a certain degree when DFT methods are applied to covalent systems. But the uncorrected DFT methods have not met equal success in

describing weak interactions and a dispersion correction has to be made in this case. The DFT-D1 approach can give satisfactory results not only for small noncovalent systems [45] but also for large ones [47, 55]. The application of the dispersion-corrected DFT methods to covalent systems is a new subject and may need further investigations. Recently, a steeper damping function was adopted by Chai and Head-Gordon [72] in their ωB97X-D functional so as to avoid a double-counting of correlation effects at short range; meanwhile the functional is reparametrized in the presence of the empirical dispersion correction. This functional might be useful for the study of the present systems, but it has not been implemented in the ADF program yet.

Acknowledgments This work was supported by Award Number SC1-HL096018 from the National Heart, Lung, and Blood Institute. The content is solely the responsibility of the authors and does not necessarily represent the official views of the National Heart, Lung, and Blood Institute or the National Institutes of Health (NIH). The ADF calculations were run on a QuantumCube™ QS32-2800C computer from Parallel Quantum Solutions, LLC.

References

1. Stryer L (1981) Biochemistry, 4th edn. Freeman, New York
2. Collman JP, Brauman JI, Halbert TR, Suslick KS (1976) Nature of O_2 and CO binding to metalloporphyrins and heme proteins. Proc Natl Acad Sci USA 73:3333–3337
3. Kuriyan J, Wilz S, Karplus M, Petsko GA (1986) X-ray structure and refinement of carbon- monoxy (Fe II)-myoglobin at 1.5 Å resolution. J Mol Biol 192:133–154
4. Cheng X-D, Schoenborn BP (1991) Neutron diffraction study of carbonmonoxymyoglobin. J Mol Biol 220:381–399
5. Kachalova GS, Popov AN, Bartunik HD (1999) A steric mechanism for inhibition of CO binding to heme proteins. Science 284:473–476
6. Vojtechovsky J, Chu K, Berendzen J, Sweet RM, Schlichting I (1999) Crystal structures of myoglobin-ligand complexes at near-atomic resolution. Biophys J 77:2153–2174
7. Lim M-H, Jackson TA, Anfinrud PA (1995) Binding of CO to myoglobin from a heme pocket docking site to form nearly linear Fe-C-O. Science 269:962–966
8. Ivanov D, Sage JT, Keim M, Powell JR, Asher SA (1994) Determination of CO orientation in myoglobin by single-crystal infrared linear dichroism. J Am Chem Soc 116:4139–4140
9. Kozlowski PM, Vogel KM, Zgierski MZ, Spiro TG (2001) Steric contributions to CO binding in heme proteins: a density functional analysis of FeCO vibrations and deformability. J Porph Phthal 5:312–322
10. McMahon MT, deDios AC, Godbout N, Salzmann R, Laws DD, Le H-B, Havlin RH, Oldfield E (1998) An experimental and quantum chemical investigation of CO binding to heme proteins and model systems: a unified model based on ^{13}C, ^{17}O, and ^{57}Fe nuclear magnetic resonance and ^{57}Fe moessbauer and infrared spectroscopies. J Am Chem Soc 120:4784–4797
11. Springer BA, Sligar SG, Olson JS, Phillips GN (1994) Mechanisms of ligand recognition in myoglobin. Chem Rev 94:699–714
12. Phillips SEV, Schoenborn BP (1981) Neutron diffraction reveals oxygen-histidine hydrogen bond in oxymyoglobin. Nature 292:81–82
13. Lukin JA, Simplaceanu V, Zou M, Ho NT, Ho C (2000) NMR reveals hydrogen bonds between oxygen and distal histidines in oxyhemoglobin. Proc Natl Acad Sci USA 97:10354–10358
14. Sigfridsson E, Ryde U (1999) On the significance of hydrogen bonds for the discrimination between CO and O_2 by myoglobin. J Biol Inorg Chem 4:99–110
15. Sigfridsson E, Ryde U (2002) Theoretical study of the discrimination between O_2 and CO by myoglobin. J Inorg Biochem 91:101–115
16. Edwards WD, Weiner B, Zerner MC (1986) On the low-lying states and electronic spectroscopy of iron(II) porphine. J Am Chem Soc 108:2196–2204
17. Waleh A, Ho N, Chantranupong L, Loew GH (1989) Electronic structure of nitrosyl ferrous heme complexes. J Am Chem Soc 111:2767–2772
18. Case DA, Huynh BH, Karplus M (1979) Binding of oxygen and carbon monoxide to hemoglobin. An analysis of the ground and excited states. J Am Chem Soc 101:4433–4453
19. Hoffmann R, Chen MML, Thorn DL (1977) Qualitative discussion of alternative coordination modes of diatomic ligands in transition metal complexes. Inorg Chem 16:503–511
20. Rovira C, Kunc K, Hutter J, Ballone P, Parrinello M (1997) Equilibrium geometries and electronic structure of iron-porphyrin complexes: a density functional study. J Phys Chem A 101:8914–8925
21. Rovira C, Parrinello M (1999) Factors influencing ligand-binding properties of heme models: a first principles study of picket-fence and protoheme complexes. Chem Eur J 5:250–262
22. Vogel KM, Kozlowski PM, Zgierski MZ, Spiro TG (1999) Determinants of the FeXO (X = C, N, O) vibrational frequencies in heme adducts from experiment and density functional theory. J Am Chem Soc 121:9915–9921
23. Vogel KM, Kozlowski PM, Zgierski MZ, Spiro TG (2000) Role of the axial ligand in heme- CO backbonding; DFT analysis of vibrational data. Inorg Chim Acta 297:11–17
24. Rovira C, Parrinello M (2000) Harmonic and anharmonic dynamics of Fe-CO and Fe-O_2 in heme models. Biophys J 78:93–100
25. Rovira C, Schulze B, Eichinger M, Evanseck JD, Parrinello M (2001) Influence of the heme pocket conformation on the structure and vibrations of the Fe-CO bond in myoglobin: a QM/MM density functional study. Biophys J 81:435–445
26. Blomberg LM, Blomberg MRA, Siegbahn PEM (2005) A theoretical study on the binding of O_2, NO and CO to heme proteins. J Inorg Biochem 99:949–958
27. De Angelis F, Jarzecki AA, Car R, Spiro TG (2005) Quantum chemical evaluation of protein control over heme ligation: CO/O_2 discrimination in myoglobin. J Phys Chem B 109:3065–3070
28. Strickland N, Mulholland AJ, Harvey JN (2006) The Fe-CO bond energy in myoglobin: a QM/MM study of the effect of tertiary structure. Biophys J 90:L27–L29
29. Scherlis DA, Cococcioni M, Sit P, Marzari N (2007) Simulation of heme using DFT + U: a step toward accurate spin-state energetics. J Phys Chem B 111:7384–7391
30. Strickland N, Harvey JN (2007) Spin-forbidden ligand binding to the ferrous-heme group: ab initio and DFT studies. J Phys Chem B 111:841–852
31. Chen H, Ikeda-Saito M, Shaik S (2008) Nature of the Fe-O_2 bonding in oxy-myoglobin: effect of the protein. J Am Chem Soc 130:14778–14790
32. Siegbahn PEM, Blomberg MRA, Chen S-L (2010) Significant van der Waals effects in transition metal complexes. J Chem Theory Comput 6:2040–2044
33. Cole DJ, O'Regan DD, Payne MC (2012) Ligand discrimination in myoglobin from linear-scaling DFT + U. J Phys Chem Lett 3:1448–1452
34. Olson JS, Phillips GN (1997) Myoglobin discriminates between O_2, NO, and CO by electrostatic interactions with the bound ligand. J Biol Inorg Chem 2:544–552

35. Krzywda S, Murshudov GN, Brzozowski AM, Jaskolski M, Scott EE, Klizas SA, Gibson QH, Olson JS, Wilkinson AJ (1998) Stabilizing bound O_2 in myoglobin by Valine68 (E11) to asparagine substitution. Biochemistry 37:15896–15907
36. Draghi F, Miele AE, Travaglini-Allocatelli C, Vallone B, Brunori M, Gibson QH, Olson JS (2002) Controlling ligand binding in myoglobin by mutagenesis. J Biol Chem 277:7509–7519
37. Coyle CM, Vogel KM, Rush TS, Kozlowski PM, Williams R, Spiro TG, Dou Y, Ikeda-Saito M, Olson JS, Zgierski MZ (2003) FeNO structure in distal pocket mutants of myoglobin based on resonance Raman spectroscopy. Biochemistry 42:4896–4903
38. Kundu S, Blouin GC, Premer SA, Sarath G, Olson JS, Hargrove MS (2004) Tyrosine B10 inhibits stabilization of bound carbon monoxide and oxygen in soybean leghemoglobin. Biochemistry 43:6241–6252
39. Chen O, Groh S, Liechty A, Ridge DP (1999) Binding of nitric oxide to iron(II) porphyrins: radiative association, blackbody infrared radiative dissociation and gas-phase association equilibrium. J Am Chem Soc 121:11910–11911
40. Momenteau M, Reed CA (1994) Synthetic heme-dioxygen complexes. Chem Rev 94:659–698
41. Spiro TG, Kozlowski PM (2001) Is the CO adduct of myoglobin bent, and does it matter? Acc Chem Res 34:137–144
42. Jung Y, Head-Gordon M (2006) A fast correlated electronic structure method for computing interaction energies of large van der Waals complexes applied to the fullerene-porphyrin dimer. Phys Chem Chem Phys 8:2831–2840
43. Sinnokrot MO, Sherrill CD (2006) High-accuracy quantum mechanical studies of pi-pi interactions in benzene dimers. J Phys Chem A 110:10656–10668
44. Hesselmann A, Jansen G, Schütz M (2005) Density-functional theory-symmetry-adapted intermolecular perturbation theory with density fitting: a new efficient method to study intermolecular interaction energies. J Chem Phys 122:14103–14120
45. Grimme S (2004) Accurate description of van der Waals complexes by density functional theory including empirical corrections. J Comput Chem 25:1463–1473
46. Riley KE, Pitonak M, Jurecka P, Hobza P (2010) Stabilization and structure calculations for noncovalent interactions in extended molecular systems based on wave function and density functional theories. Chem Rev 110:5023–5063
47. Liao M-S, Huang M-J, Watts JD (2012) Assessment of dispersion corrections in DFT calculations on large biological systems. Mol Phys 110:3061–3076. doi:10.1080/00268976.2012.695811
48. Grimme S, Antony J, Ehrlich S, Krieg H (2010) A consistent and accurate ab initio parametrization of density functional dispersion correction (DFT-D) for the 94 elements H-Pu. J Chem Phys 132:154104–1-25
49. Grimme S, Ehrlich S, Goerigk L (2011) Effect of the damping function in dispersion corrected density functional theory. J Comput Chem 32:1456–1465
50. Steinmann SN, Corminboeuf C (2011) Comprehensive benchmarking of a density- dependent dispersion correction. J Chem Theory Comput 7:3567–3577
51. Springer BA, Egeberg KD, Slighar SG, Rohlfs RJ, Mathews AJ, Olson JC (1989) Discrimination between oxygen and carbon monoxide and inhibition of autooxidation by myoglobin. Site-directed mutagenesis of the distal histidine. J Biol Chem 264:3057–3060
52. Radon M, Pierloot K (2008) Binding of CO, NO, and O_2 to heme by density functional and multireference ab initio calculations. J Phys Chem A 112:11824–11832
53. Traylor TG, Stynes DV (1980) Isocyanide binding to chelated protoheme. Kinetic criteria for distal steric effects in hemoproteins. J Am Chem Soc 102:5938–5939
54. Grimme S (2006) Semiempirical GGA-type density functional constructed with a long-range dispersion correction. J Comput Chem 27:1787–1799
55. Liao M-S, Watts JD, Huang M-J (2009) Dispersion-corrected DFT calculations on C_{60}-porphyrin complexes. Phys Chem Chem Phys 11:4365–4374
56. Liao M-S, Huang M-J, Watts JD (2010) Iron porphyrins with different imidazole ligands – a theoretical comparative study. J Phys Chem A 114:9554–9569
57. Quillin ML, Arduini RM, Olson JS, Phillips GN (1993) High-resolution crystal structures of distal histidine mutants of sperm whale myoglobin. J Mol Biol 234:140–155
58. te Velde G, Bickelhaupt FM, van Gisbergen SJA, Fonseca-Guerra C, Baerends EJ, Snijders JG, Ziegler T (2001) Chemistry with ADF. J Comput Chem 22:931–967
59. ADF2012.01. SCM, Theoretical Chemistry, Vrije Universiteit, Amsterdam, Netherlands. See also (http://www.scm.com)
60. Becke AD (1988) Density-functional exchange-energy approximation with correct asymptotic behavior. Phys Rev A 38:3098–3100
61. Perdew JP (1986) Density-functional approximation for the correlation energy of the inhomogeneous electron gas. Phys Rev B 33:8822–8824
62. Perdew JP, Burke K, Ernzerhof M (1996) Generalized gradient approximation made simple. Phys Rev Lett 77:3865–3868
63. Zhang Y-K, Yang W-T (1998) Comment on "Generalized gradient approximation made simple". Phys Rev Lett 80:890–890
64. Becke AD (1993) Density-functional thermochemistry.3. The role of exact exchange. J Chem Phys 98:5648–5652
65. Lee C, Yang WT, Parr RG (1988) Development of the colle-salvetti correlation-energy formula into a functional of the electron-density. Phys Rev B 37:785–789
66. Liao M-S, Huang M-J, Watts JD (2011) FeP(Im)-AB bonding energies evaluated with a large number of density functionals (P = porphine, Im = imidazole, AB = CO, NO, and O_2). Mol Phys 109:2035–2048
67. Kannemann FO, Becke AD (2010) van der Waals interactions in density-functional theory: intermolecular complexes. J Chem Theory Comput 6:1081–1088
68. Tang KT, Toennies JP (1984) An improved simple model for the van der Waals potential based on universal damping functions for the dispersion coefficients. J Chem Phys 80:3726–3741
69. Barone V, Biczysko M, Pavone M (2008) The role of dispersion correction to DFT for modelling weakly bound molecular complexes in the ground and excited electronic states. Chem Phys 346:247–256
70. Ziegler T, Tschinke V, Baerends EJ, Snijders JG, Ravenek W (1989) Calculation of bond energies in compounds of heavy elements by a quasi-relativistic approach. J Phys Chem 93:3050–3056
71. Jameson GB, Molinaro FS, Ibers JA, Collman JP, Brauman JI, Rose E, Suslick KS (1980) Models for the active site of oxygen-binding hemoproteins. Dioxygen binding properties and the structures of (2-methylimidazole)-meso-tetra(alpha, alpha, alpha, alpha-o-pivalamidophenyl)porphyrinatoiron(II)-ethanol and its dioxygen adduct. J Am Chem Soc 102:3224–3237
72. Chai J-D, Head-Gordon M (2008) Long-range corrected hybrid density functionals with damped atom–atom dispersion corrections. Phys Chem Chem Phys 10:6615–6620